Funded by the Horizon 2020 Framework Programme of the European Union
Grant Agreement No. 871158

AHEAD 2020 Scientific/Technical Report - WP 9.8

Understanding the interaction between soft protons and X-ray mirrors

Final report

Reference Period: 02/03/2020 – 01/09/2022

V.Fioretti[1], T. Mineo[2], R. Amato[2], S. Lotti[3], C. Macculi[3], S. Molendi[4], F. Gastaldello[4], G. Lanzuisi[1], M. Cappi[1], M. Dadina[1], S. Ettori[1]

[1]INAF OAS Bologna, [2]INAF IASF Palermo, [3]INAF IAPS Roma, [4]INAF IASF Milano

Project acronym:
AHEAD2020

Version: 1.2
Date: 3/10/2022

Project Title:
Integrated Activities for the High Energy Astrophysics Domain

Grant Agreement No: **871158**
This deliverable is part of a project that has received funding from the European Union's Horizon 2020 research and innovation programme

Start date of the project:
2020-03-02

Version	Revision Date	Review/Approval
1.0	1/09/2022	Creation date
1.1	3/10/2022	Internal review
1.2	14/10/2022	Included comments by WP leaders

Distribution List	Date	Version
AHEAD2020 WP 9	5/10/2022	1.1
AHEAD2020 WP 9	14/10/2022	1.2

0. Explanation of the work carried out within the WP 4
0.1 Activity breakdown **Error! Bookmark not defined.**
1. XMM-Newton proton response matrix design (Task 1) **Error! Bookmark not defined.**
1.1 EPIC soft proton spectra extraction (Task 1.1) **Error! Bookmark not defined.**
1.2 Geant4 XMM soft proton scattering (Task 1.2) **Error! Bookmark not defined.**
1.3 Ray-tracing XMM soft proton scattering (Task 1.3) **Error! Bookmark not defined.**
1.4 Geant4 proton attenuation simulation (Task 1.4) **Error! Bookmark not defined.**
1.4.1 MOS focal plane assembly **Error! Bookmark not defined.**
1.4.2 PN focal plane assembly **Error! Bookmark not defined.**
2. ATHENA proton response matrix design (Task 2) 5
2.1 Geant4 ATHENA soft proton scattering (Task 2.1) 5
2.2 Ray-tracing ATHENA soft proton scattering (Task 2.2) 6
2.3 Geant4 X-IFU proton scattering simulation (Task 2.3) 8
2.4 Geant4 WFI proton scattering simulation (Task 2.4) 9
3. Data formatting, verification and validation (Task 3) 11
3.1 Data input formatting (Task 3.1) 11
3.2 XMM-Newton and ATHENA proton response matrix (Task 3.2) 11
3.3 Verification of the XMM-Newton and ATHENA response files (Task 3.3) 15
3.4 Validation of the XMM-Newton proton response files (Task 3.4) 17
3.4.1 Validation with single observations 17
3.4.2 Validation with orbit averaged spectra 20
3.4.3 Summary of the validation activity 21
References 21
Deliverables 24
Dissemination & communication activities 25
Deviations and non-compliances 26

2. ATHENA proton response matrix design (Task 2)

The ATHENA space telescope is the future ESA L-class X-ray mission [23], designed to address the Cosmic Vision "The Hot and Energetic Universe" science theme. With a planned launch in the 2030s in an L1 orbit, ATHENA will carry an X-ray modular mirror based on Silicon Pore Optics (SPO) technology with a focal length of 12 m and an unprecedented effective area of 1.4 m^2 at 1 keV. Two instruments populate the focal plane, covering the soft < 15 keV energy range: a Wide Field Imager (WFI [24]) for wide field imaging and spectroscopy and an X-ray Integral Field Unit (X-IFU [25]) for fine X-ray spectroscopy.

Geant4 simulations of the soft proton-induced background at both detectors [26, 27] have proved that soft protons threaten the achievement of the ATHENA scientific requirements. For this reason, a magnetic diverter has been designed to shield the focal plane from charged particles entering the field of view, and simulations for the focused background drove its specifications.

Because of the complexity and large diameter of the mirror, both Geant4 and ray-tracing simulations of the proton scattering effect require significant CPU running times to get a minimum statistical level, so testing different input models and exploring different requirements for the diverter is practically impossible. The ATHENA proton response files will provide fast evaluations of the soft proton-induced background level - without the magnetic diverter - to optimize the diverter design and better characterize the focused background.

2.1 Geant4 ATHENA soft proton scattering (Task 2.1)

The Athena SPO proton scattering efficiency was extensively evaluated [27] during the ESA AREMBES project with independent mirror models built using Geant4 and ray-tracing simulation frameworks, with a systematic difference in the efficiency of about 20% using the same scattering model. In the meantime, a new SPO design was released [28] with a different mirror module layout and a rib pitch of 2.3 mm. The Geant4 mass model delivered by the AREMBES project [10] was updated to a rib pitch of 2.3 mm according to the most recent SPO design. The effect of the new layout was introduced as a normalization factor in the ARF based on the results obtained with the ray-tracing simulator (Sect. 2.2). The geometry uses a truncated cone to emulate the paraboloid and hyperboloid stacks of the mirror modules, with a total of modular 15 rows built in the Geant4 code [Fig. 15]. No coating is applied to the reflecting surface because simulations performed in the past indicated a difference in the scattering efficiency by a few percent. The Single Scattering model is used to model the proton interaction with the mirror surface.

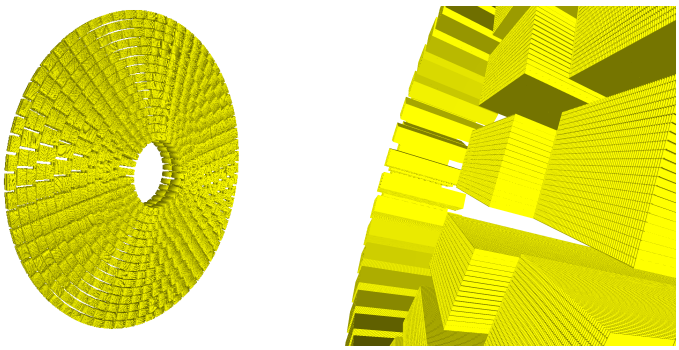

Figure 15: Geant4 mass model of the updated ATHENA SPO.

2.2 Ray-tracing ATHENA soft proton scattering (Task 2.2)

Th optics are simulated as concentric shells (one for each plate) with pores and multiple reflections inside pores are not considered. Both the new rib pitch and mirror layout were included in the updated simulation. The proton scattering physics interaction uses the Remizovich model in non-elastic approximation. The new mirror geometry has been implemented in the code and verified by comparing the on-axis X-ray photon transmission from a point source with the X-ray effective area and vignetting presented in the SPO ESA report [28]. Fig. 16 shows the agreement between the current ray-tracing simulation and the SPO performance.

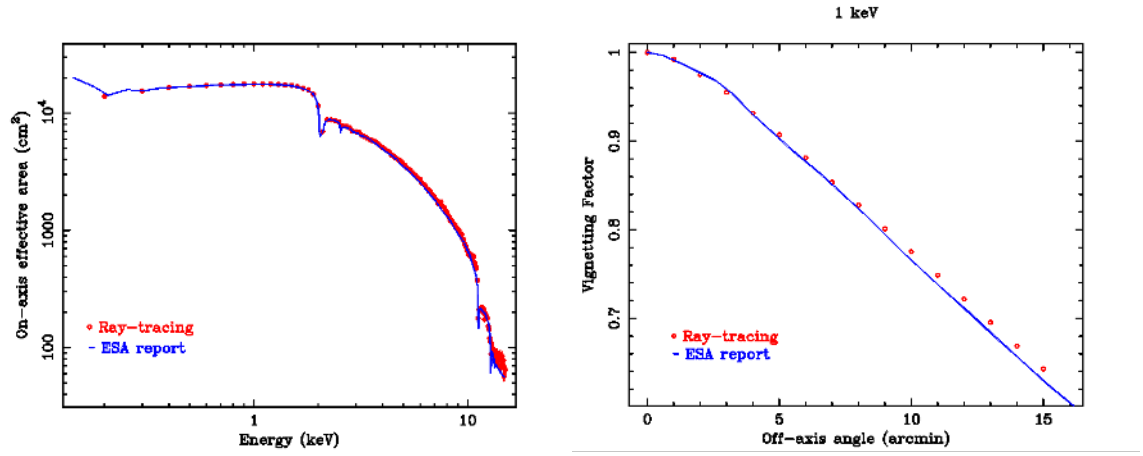

Figure 16: (left) On-axis effective area for a point source as a function of the photon energy: the red dots are values obtained from the ray-tracing, and the blue line is the curve presented in the ESA report. (right) The vignetting factor for 1 keV input photons as a function of the input angles: the red dots are values obtained from the ray-tracing, and the blue line is the curve presented in the ESA report.

We simulated the proton flux at the focal plane, defined as a circular region with a radius of 10 cm, using the Geant4 (Single Scattering) and Ray-tracing (Remizovich) simulators. We compared the spectral and radial distributions, and the transmission factor T defined as:

$$T = \frac{N_{out} \times \Omega_{in} \times A_{SPO}}{N_{in} \times 4\pi \times A_{FP}}$$

where N_{in} and N_{out} are the input and exiting protons, Ω_{in} is the input cone solid angle, A_{SPO} and A_{FP} are the SPO surface and the 10 cm radius focal plane respectively.

With the new rib pitch of 2.3 mm, we obtain:

- Geant4 T (old layout): 4.6×10^{-5};
- Ray-tracing T:
  - old layout: 9.9×10^{-5} (2x Geant4);
  - new layout: 1.5×10^{-4} (3x Geant4, given by the 2x factor for the different physics model and the 1.5x factor for the layout).

In terms of efficiency, the new mirror layout increments the proton effective area by a 1.5 factor, while keeping the same spectral and angular distribution. Fig 17 shows the proton spectra obtained at the focal plane, with the left panel referring to the new layout and the right panel to the old one. Fig. 18 computes for a set of radial annuli from the center of the focal plane the mean proton angle w.r.t. the telescope axis. Thanks to this consistency, a 1.5 incremental factor was added to the Geant4 ARF files without the need to build a new Geant4 mass model of the ATHENA SPO.

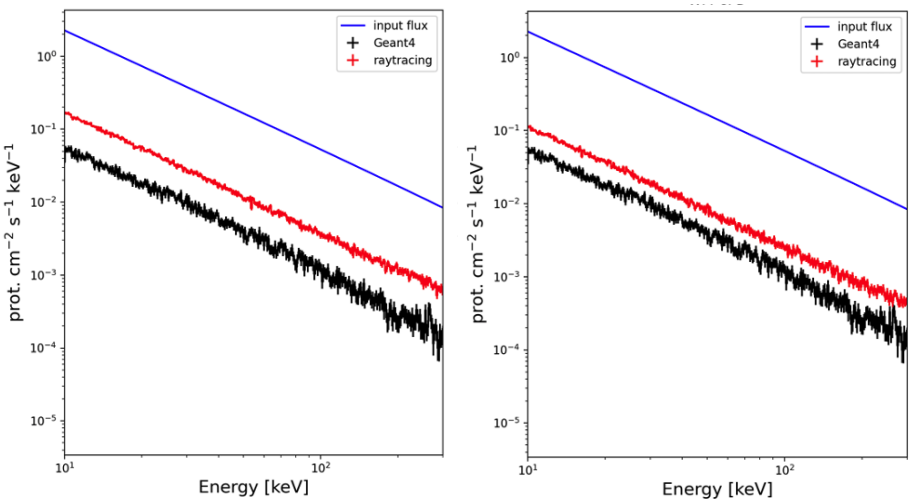

Figure 17: The Geant4 and ray-tracing simulated proton spectra at the 10 cm radius focal plane after scattering with the SPO. From left to right, the ray-tracing uses the new and old SPO mirror module layout.

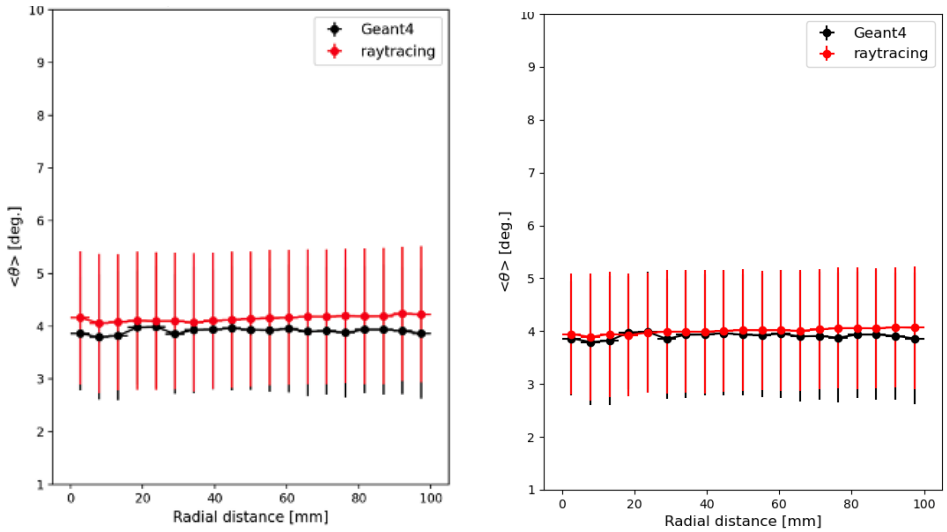

Figure 18: The Geant4 and ray-tracing simulated mean proton angle along the radial distribution at the 10 cm radius focal plane after scattering with the SPO. From left to right, the ray-tracing uses the new and old SPO mirror module layout.

2.3 Geant4 X-IFU proton scattering simulation (Task 2.3)

The Geant4 mass model of the X-IFU FPA was provided by the ATHENA X-IFU instrument background working group and a detailed description can be found in [29]. The mass model includes the set of fixed thermal filters placed within the cryostat aperture cylinder at the top of the detector according to the latest design. We will refer to the X-IFU filters as Optical Blocking Filters (OBF) for consistency with the WFI design. The proton detection efficiency within the 0.2 - 12.5 keV energy range is shown in Fig. 19. We note that a long tail extends to the energy upper limit and that at 300 keV there is still a non-negligible fraction of protons that is detected by the X-IFU, even if with an efficiency more than 10 times lower than the peak. This is likely caused by multiple secondary scattering within the aperture cylinder, with protons losing energy at each scattering with the inner surface.

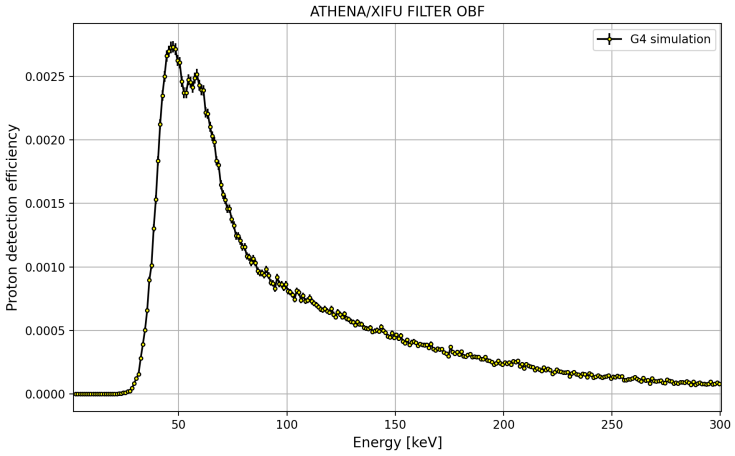

Figure 19: X-IFU FPA proton detection efficiency.

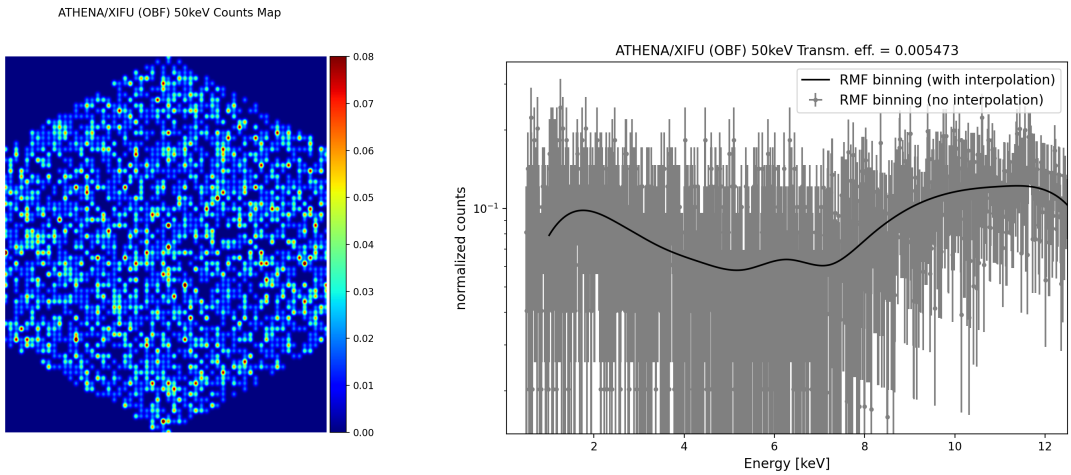

Figure 20: X-IFU counts map (left) and interpolation of the spectral distribution (right) for an input energy of 50 keV at the mirror entrance.

The input protons used for the FPA are extracted at the aperture cylinder entrance at 388 mm from the detector. The proton lists were first modelled in angular and energy distribution and then randomly generated for the EPIC simulation.

The same event reconstruction described for the MOS in Sect. 1.4.1 was used for the ATHENA instruments. The X-IFU counts map, in the 0.2 - 12.5 keV energy range, is shown in Fig 20 (left) for an input proton energy of 50 keV. The RMF for the X-IFU uses the same pipeline of XMM, with the energy spectrum first re-binned and interpolated, and then the interpolation function filling a reduced set of channels (Fig. 20, right) as described in Sect. 3.1.

2.4 Geant4 WFI proton scattering simulation (Task 2.4)

The WFI Geant4 mass model, built for the WFI instrument background group simulations [27], includes:

- The wide field detector itself, composed of four pixelated quadrants each with 512×512, 130×130 μm^2 side pixels, with a thickness of the Si sensor of 450 μm;
- The fixed on-chip filter covering the pixels of the four quadrants and composed, from top to bottom, of 90 nm of aluminum (Al), 30 nm of silicon nitride (Si3N4), and 20 nm of silicon oxide (SiO2);
- The squared 17×17 cm^2 Optical Blocking Filter on the filter wheel composed from top to bottom of 30 nm of Al and 150 nm of Kapton (polyimide). This filter is optional depending on the wheel position.

A squared Aluminum baffle is placed on top of the WFI. Given that the MOS proton response files are not affected, within the uncertainties, by the baffle secondary scattering we decided to extract the proton at the filter wheel height, 10 cm, and neglecting the effect of the baffle. This allowed us to increment the statistics and to better model the energy redistribution. The proton detection efficiency within the 0.2 - 15 keV energy range is shown in Fig. 21 with and without the OBF.

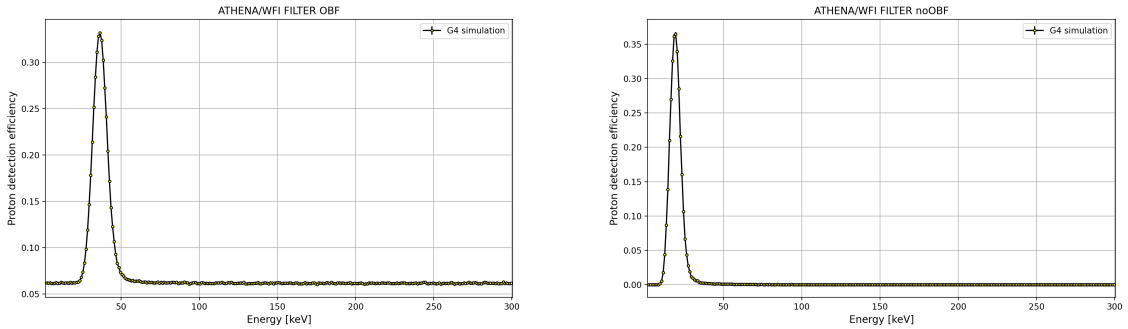

Figure 21: WFI proton detection efficiency with (left) and without (right) the OBF.

The event reconstruction is the same as the previous instruments. The WFI counts map, in the 0.2 - 15 keV energy range, is shown in Fig 22 (left) for an input proton energy of 50 keV. The RMF for the WFI uses the same pipeline of XMM, with the energy spectrum first re-binned and interpolated, and then the interpolation function filling the X-ray RMF channels (Fig. 22, right) as described in Sect. 3.1.

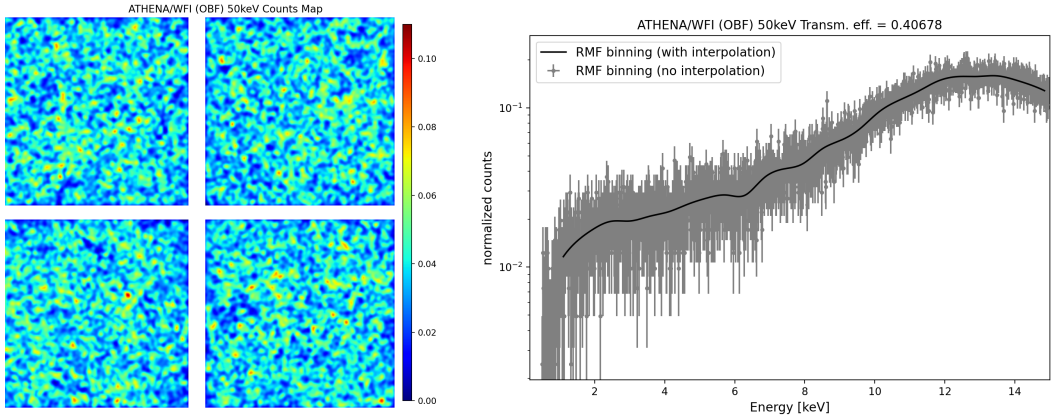

Figure 22: WFI counts map (left) and interpolation of the spectral distribution (right) for an input energy of 50 keV at the mirror entrance.

3. Data formatting, verification and validation (Task 3)

3.1 Data input formatting (Task 3.1)

The proton response files are composed by a Redistribution Matrix File (RMF) mapping the proton energy space (from few to hundreds of keV) into detector pulse heights and an Auxiliary Response File (ARF) collecting the grasp of the optics, the filter transmission efficiency and the detector quantum efficiency. The files are formatted according to the NASA OGIP (Office of Guest Investigators Program) calibration database (caldb) format, and it consist into an RMF and ARF file in FITS (Flexible Image Transport System) format. Any X-ray data analysis tool available to the X-ray astronomy community and compliant with the NASA caldb format can be used to simulate the soft proton induced background spectra, for any given condition of the orbit proton environment without the need to run again the simulation pipeline. We chose the NASA *Xspec*[1] fitting package for the verification and validation results presented in Sect. 3.3 and 3.4.

The energy distribution is binned according to the respective instrument X-ray channels, except for the X-IFU. Because of the smaller aperture and detection area, its simulation was the one that suffered the most from the limited statistics and using the original energy resolution, the smallest among the simulated detectors, was practically impossible. A binning factor of 25 was instead used.

- The EPIC cameras[2]:
  - MOS: a total of 800 channels, an energy width of 15 eV and energy boundaries of 0 – 12 keV.
  - PN: a total of 4096 channels, a mean energy width of 5 eV and energy boundaries of 0 - 20 keV.
- The ATHENA X-ray instruments[3,4]:
  - X-IFU: a total of 1196 channels, an increasing energy width from about 5 eV to about 30 eV and energy boundaries of 0.06116 - 12.49961 keV.
  - WFI: a total of 1485 channels, an energy width of 10 eV and energy boundaries of 0.15 - 15 keV.

3.2 XMM-Newton and ATHENA proton response matrix (Task 3.2)

The simulation pipeline logical schema is shown in Fig. [23]. The mirror simulation is performed with two independent simulation frameworks based on ray-tracing and the Geant4 toolkit in order to verify the geometry and physics models and estimate potential systematic effects in their implementation. Since the two simulators give comparable angular and spatial distributions of the protons at the focal plane, with only a factor 2 difference in the proton flux affecting the grasp stored in the ARF file, only the output of the Geant4 simulator, in the form of an event list, storing energy and angular distribution of the protons at a given distance from the focal plane, is extracted and given as input to a Geant4 simulation of the FPA, including baffles, optical filters and the detectors. From the FPA simulation, we reconstruct the counts on the XMM-Newton and ATHENA detectors, applying a pattern flag, according to the instrument read-out

[1] https://heasarc.gsfc.nasa.gov/xanadu/xspec/

[2] https://www.cosmos.esa.int/web/xmm-newton/epic-response-files

[3] http://x-ifu-resources.irap.omp.eu/PUBLIC/RESPONSES/CC_CONFIGURATION/

[4] https://www.mpe.mpg.de/ATHENA-WFI/public/resources/responses/

configuration, and a baffle flag for the protons that interact with the radiation shielding before reaching the detector. The product of this processing stage is a data level 1 FITS file listing the count energy, position, pattern and baffle flags, one for each Geant4 simulation run of each input energy. In data level 2 we compute for each input energy the energy probability distribution in the instrument channels, normalized to 1, and the grasp. For X-ray photons, that are mono-directional, the response ARF file is the product of the effective area of the mirror, i.e. geometric area multiplied by the reflection efficiency, the filter transmission efficiency and the detector quantum efficiency. For the soft proton environment, we assume an isotropic distribution at the mirror entrance and the input aperture angle used in the simulation must be taken into account when computing the total transmission efficiency. The simulated grasp is the product of the system efficiency multiplied by the proton aperture solid angle at the mirror entrance, in units of cm^2 sr. The data level 2 files are then unified and formatted into the OGIP RMF and ARF response files. A different proton response will be produced for each combination of mirror simulator, optical filter type, and focal plane instrument.

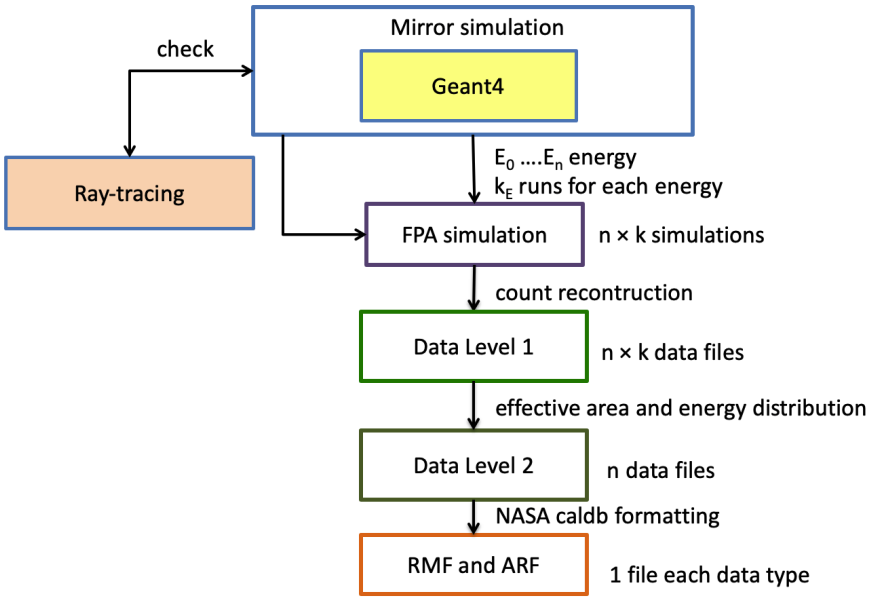

Figure 23: Logical schema of the software pipeline generating the response files.

The pattern analysis shows that 99.9% of the simulated counts has a pattern of 0, i.e. only one pixel triggered for each event, as in the in-flight focused non X-ray background. For this reason, all the proton response files were produced selecting only singles (PATTERN = 0 for the EPIC cameras). We note here that the PATTERN terminology was also used for ATHENA since its terminology and selection criteria are still unknown.

At first, we planned to connect the FPA to the mirror simulation by using the same proton list at the mirror output as input for the FPA simulation. This allows to reproduce the exact same angular, spatial and energy distribution. However, the CPU simulation time required to achieve a minimum statistical level to model the energy distribution turned out to be unfeasible (6 months for XMM, more than 1 year for ATHENA). The solution was to model the angular and energy distribution of the protons at the input of the FPA simulation and then exploit the Geant4 Monte Carlo generator to randomly sample the protons within the modelled distribution. There are several assumptions in this approach: (i) the protons are spatially uniform when reaching the FPA, (ii) the angular distribution is spatially uniform, (iii) there is no dependence among the proton energy, angle and the position. Selecting the MOS as a use case, we tested that at a height of 754

mm (the baffle entrance) both the assumptions (i) and (ii) can be considered valid, within the statistical uncertainties, as shown in Fig. 24 (for a 50 keV input proton energy).

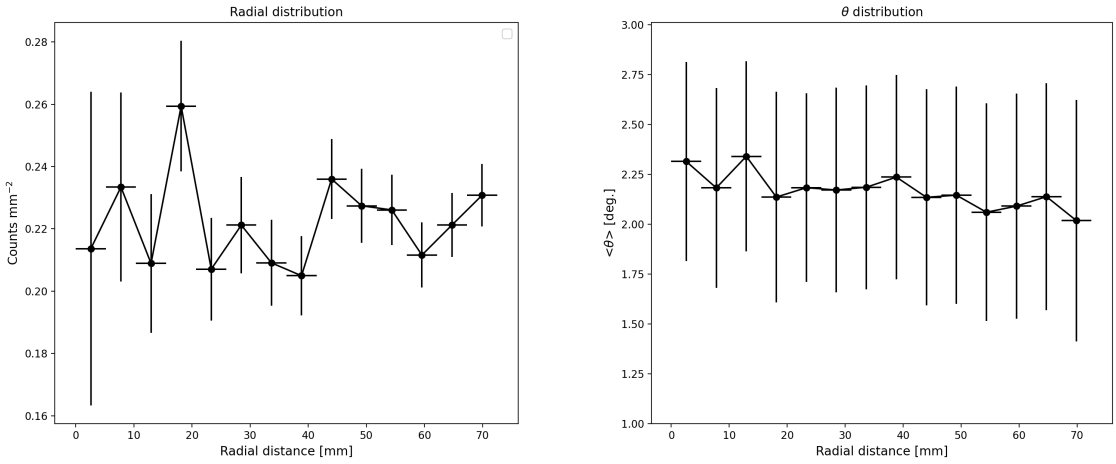

Figure 24: Radial distribution (left) and radial distribution of the mean angular distribution w.r.t. the normal (right) of the protons exiting the XMM mirror and entering the baffle at 754 mm from the MOS.

To test the third assumption, i.e. to assess that we did not introduce any biases in the approximations of the modelled proton distribution, we produced two simulated background spectra, one obtained with the proton list and one with the modelled distribution (Fig. 25). The resulting spectra are comparable, despite the limited statistics of the spectrum using the proton lists as input.

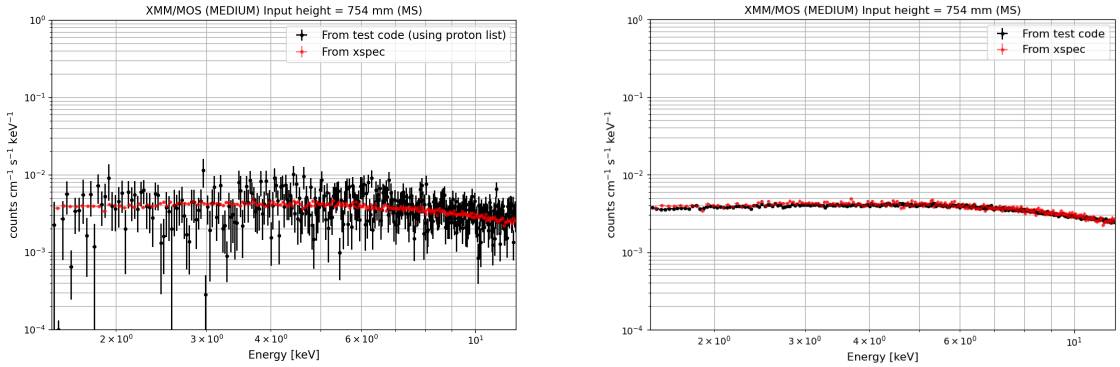

Figure 25: Comparison of simulated background spectra, in black, using proton lists (left) or models (right). The simulation obtained with the final proton response file is shown in red.

The resulting energy redistribution matrix, plotted as incident vs measured energy and stored in the RMF files, is shown in Fig 26 and 27 (medium filter for the EPIC cameras and with OBF for the WFI). For each input proton energy (Y-axis), the RMF stores the energy distribution detected by the instruments (X-axis) normalized to 1. The presence of the two peaks in the MOS transmission efficiency is clearly visible. The RMFs and ARFs files are averaged on the camera field of views.

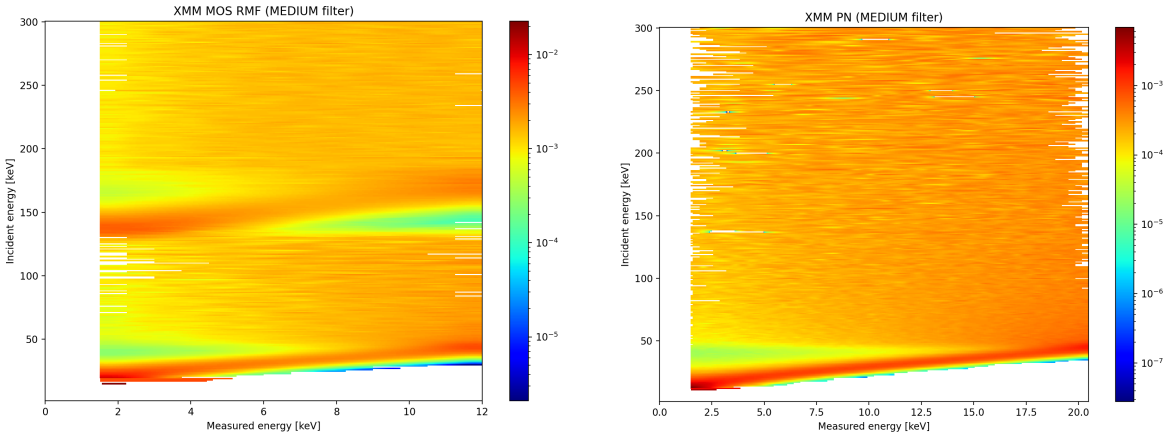

Figure 26: Plot of the RMF for the EPIC MOS and PN CCDs (medium filter

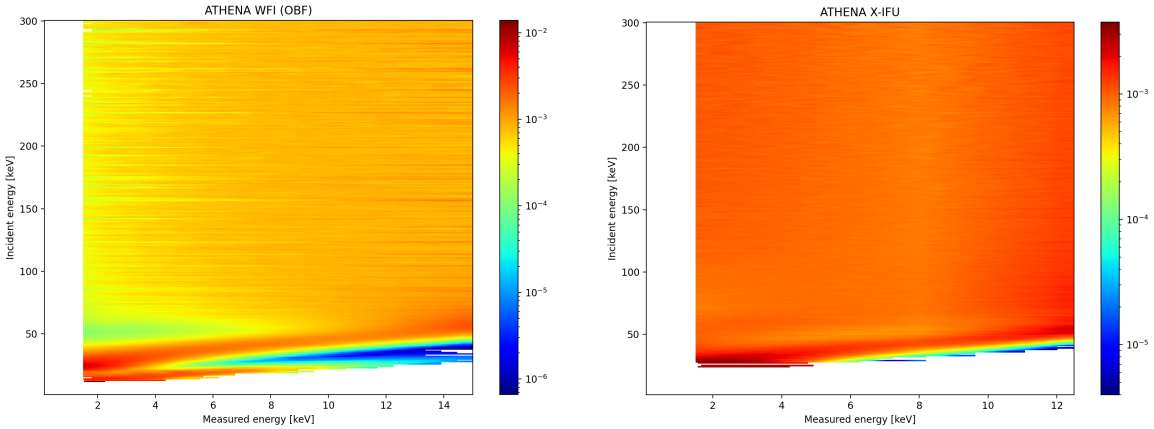

Figure 27: Plot of the RMF for the ATHENA WFI (with OBF) and X-IFU detectors.

The validity energy ranges, required to avoid artefacts by the interpolation model and defined by the comparison with standard simulations (see Sect 3.3) are:

- The EPIC cameras:
  - MOS: 1.5 - 11.5 keV
  - PN: 1.5 - 19.5 keV
- The ATHENA X-ray instruments:
  - X-IFU: 1.5 - 7 keV (the limited upper energy threshold is due to the lower statistics achieved in the X-IFU Geant4 simulations because of the intrinsic lower soft proton induced background flux)
  - WFI: 1.5 - 11.5 keV

The user should ignore the channels outside the validity ranges when performing their analysis.

Considering the 15-20% systematic uncertainty in the mirror simulation, the approximation (< 20%) introduced by sampling models of the proton list at the FPA input, and considering the factor 2 of difference between the Geant4 and ray-tracing simulated effective area, we assign a total uncertainty of 50% to the simulations obtained with the proton response files, to which the user must sum the errors in the input models.

3.3 Verification of the XMM-Newton and ATHENA response files (Task 3.3)

The verification of the proton response files consisted in checking their technical correctness by simulating the X-ray background spectrum with *Xspec* using the proton response files, as a general user would do, and in parallel using the L1 data files that store a list of counts for each input energy, to obtain a "standard" simulation where a model is used as input at the mirror entrance and the background is obtained by collecting the counts at the detector.

We chose as input models two proton spectral distributions based on in-flight measurements and representative of very different environments: the interplanetary solar wind (SW) that spacecrafts encounter when operating outside the Earth's magnetosphere, and the magnetosheath (MS), a plasma regime of the magnetosphere lying behind the bow shock boundary layer in the magnetotail up to the L2 region. The protons models for the MS and SW were extracted in [26] to simulate the ATHENA soft proton-induced background in L1 and L2. They refer to an active state of the magnetosphere and the maximum flux encountered in 90% of the operational time. Given the highly elliptical orbit of XMM-Newton, crossing both regions inside and outside the magnetosphere, these models can also represent the soft proton fluxes potentially producing the XMM's flares. The input proton models are shown in Fig. 28. While the uncertainties for the MS model are based on the AREMBES reported uncertainties, for the SW, for which more extended observations were available, we assumed a standard 20%. We must note that both models were produced from observations starting at about 50 keV (47 keV for the SW and 58 keV for the MS) and then extrapolated to lower energies. No actual measurements are available in the very soft proton regime.

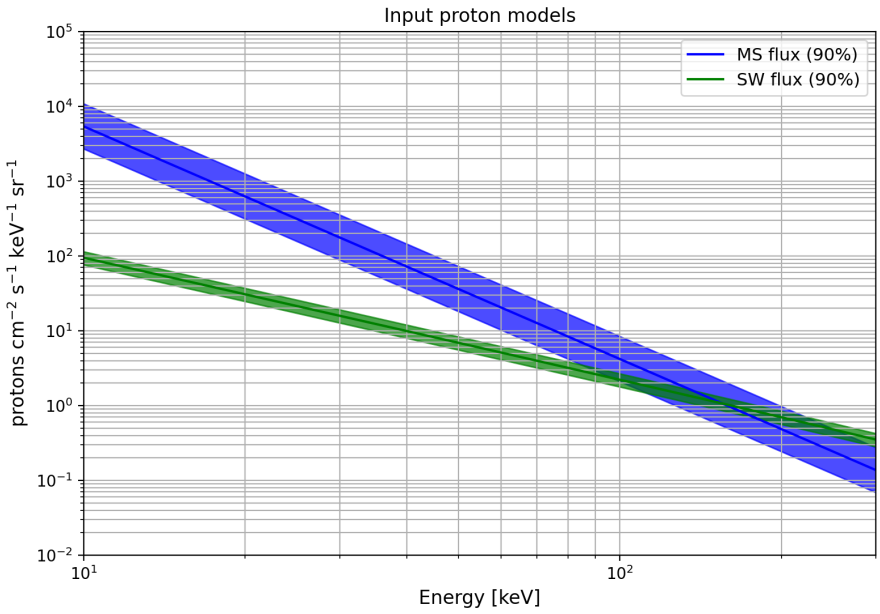

Figure 28: Proton spectral models used as input in the verification and validation activity.

In *Xspec*, the background flux, in cts cm^{-2} s^{-1} keV^{-1}, is obtained by convolving the input model with the RMF and ARF files. We note that since the ARF stores the grasp of the telescope, the input model is in *steradiant* units. The standard simulation is done by computing the simulated exposure to the input flux and dividing by the energy bins. Both spectra are normalised for the detector area. The result is shown in

Fig. 29 - 32 for the MS (left) and the SW (right) input models. The same background spectra are predicted from the standard simulation method and the use of the proton response files produced by this work.

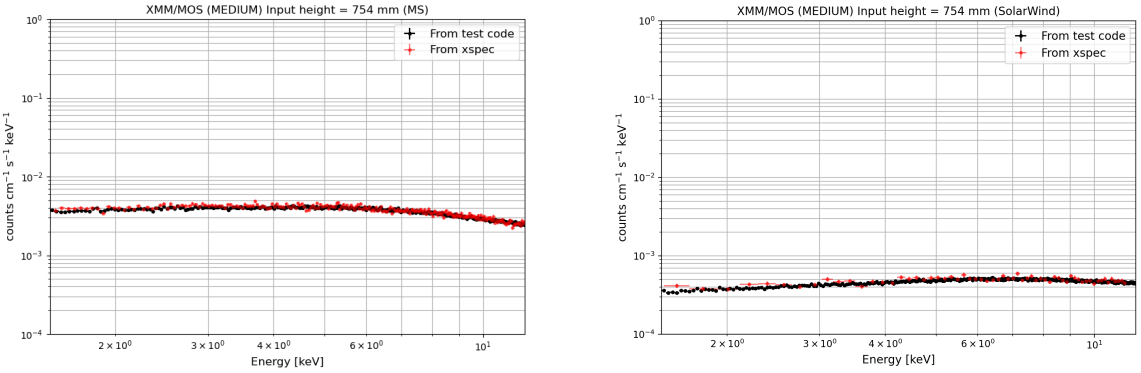

Figure 29: Comparison between a MOS standard simulation, using a power-law in input and obtained with *Xspec* using the proton response files, for an MS (left) and SW (right) input model.

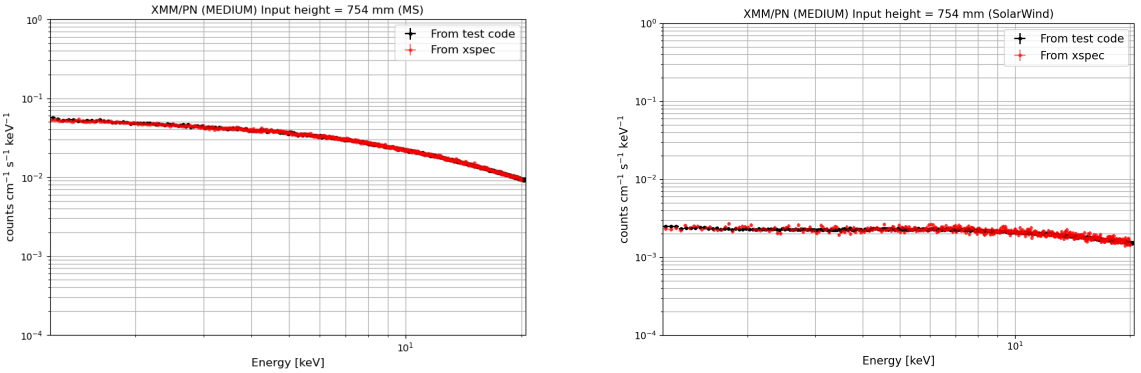

Figure 30: Comparison between a PN standard simulation, using a power-law in input, and obtained with *Xspec* using the proton response files, for an MS (left) and SW (right) input model.

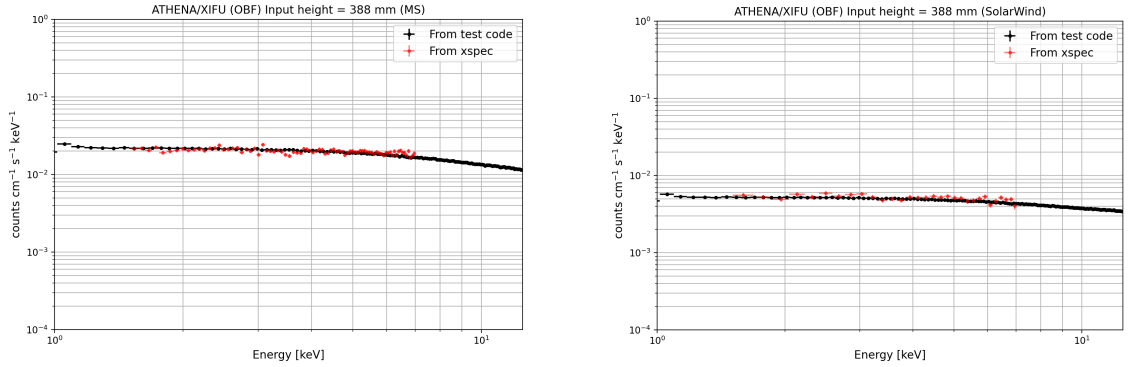

Figure 31: Comparison between an X-IFU standard simulation, using a power-law in input, and obtained with *Xspec* using the proton response files, for an MS (left) and SW (right) input model.

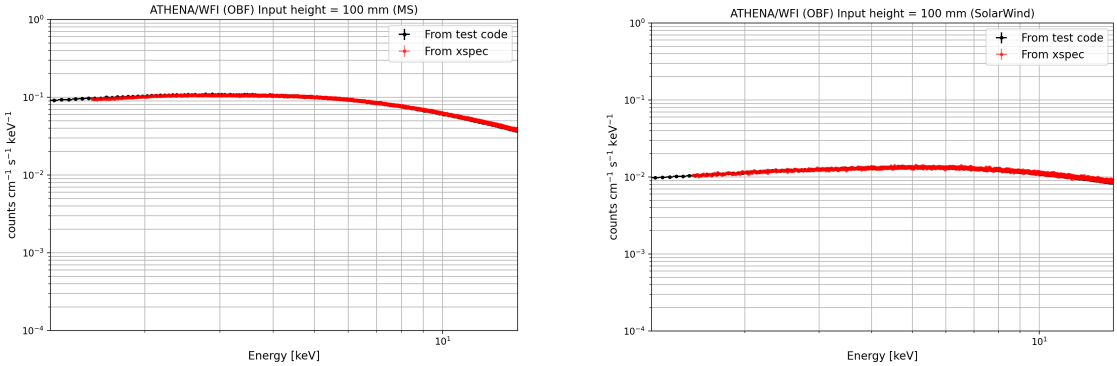

Figure 32: Comparison between a WFI standard simulation, using a power-law in input, and obtained with *Xspec* using the proton response files, for an MS (left) and SW (right) input model.

3.4 Validation of the XMM-Newton proton response files (Task 3.4)

The proton response matrices produced with the telescope end-to-end simulation need to be validated using real data. To this purpose, two kinds of analysis have been performed: the first considers data from single observations where both PN and MOS were available, and the second uses a representative MOS spectrum for the maximum rate expected in 90% of observation time, obtained from 12 years of observations (see Sect. 1.1).

3.4.1 Validation with single observations

Data from each considered set are reduced following the standard procedure using the XMM-Newton Science Analysis System (SAS v. 19.0.1). The MOS and PN data were processed with *emproc* and *epproc* tasks respectively and “Single” (PATTERN=0) pixel event patterns were selected for both detectors to be compliant with the proton response matrices.
Soft proton (SP) counts were extracted without any spatial selection using light curves in time bins of 100 s to identify the period where high background levels contaminated the scientific observation. Intervals

with rate > 10 c/s for PN and > 3 c/s for MOS were considered for the flare spectra accumulation. The background spectra were accumulated, identifying the time interval suitable for scientific observations of X-ray sources in the field of view. In particular, the intervals considered are those where the PN rate was < 4 c/s and where the MOS rate was < 2 c/s for ID 0000110101 and < 1 c/s for ID 0049150301 and ID 0864330201. Fig. 29 shows the flare (blue rectangle) and background intervals (red rectangle) selected for the analysis of ID 0049150301.
Information on the observations considered for this analysis is shown in Table 3. The energy range considered for the analysis is 2.0-11.5 keV.

	ID 0000110101		**ID 00049150301**		**ID 0864330201**	
Obs. Date	2001-08-19		2002-06-16		2020-01-10	
Duration (s)	15505		8250		141000	
Filter	MEDIUM		THIN1		THIN1	
	PN (c/s)	MOS(c/s)	PN (c/s)	MOS(c/s)	PN (c/s)	MOS (c/s)
SP Rate*	34.7	8.17	62.9	15.5	69.45	8.66
Bkg rate*	1.70	0.58	1.32	0.37	2.43	0.61

*The rate is computed in the energy range 2.0-11.5 keV.

Table 3: Log of the observations used for the analysis

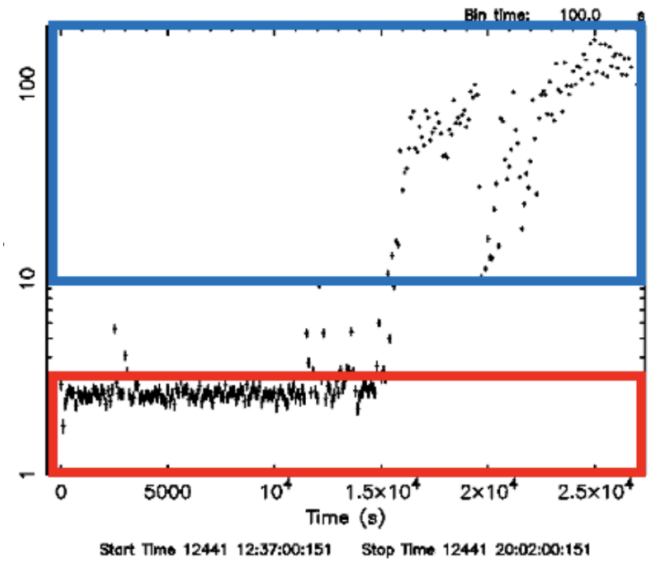

Figure 29: Light curve relative to PN observation of ID 0049150301 binned in 100 seconds. The blue and red rectangles identify the time interval used to collect soft protons and the background spectra, respectively.

From the spectral analysis, the following points have been derived:

- A single power law is not able to fit the entire energy range 2.0-11.5 keV either for MOS or PN in none of the observations. Fig. 30 shows, as an example, the fitting relative to the PN spectrum of ID 0000110101.
- A single power law is able to fit the range 5-11.5 keV in both observations with a spectral index 20±1% higher in the MOS with respect to the PN. The discrepancy between MOS and PN increases to 60% in the lower range 2-5 keV with the MOS steeper than the PN.

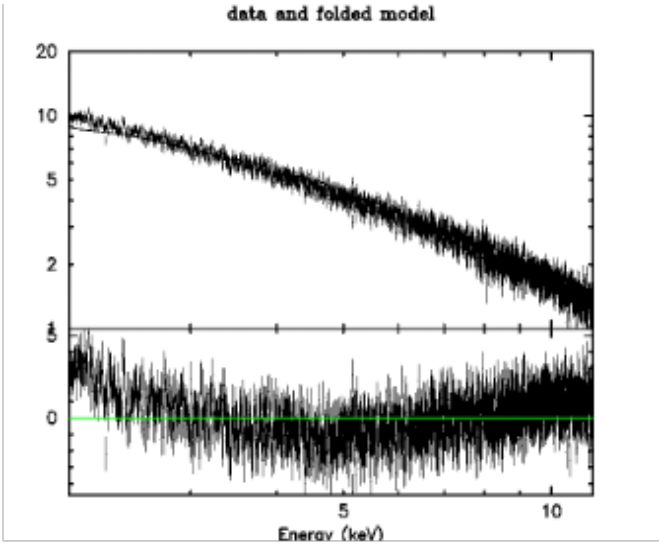

Figure 30: Fit with a single power-law of the ID 0000110101 PN spectrum.

	00049150301			**0000110101**			**ID 0864330201**		
	PN	MOS	MOS/ PN	PN	MOS	MOS/ PN	PN	MOS	MOS/ PN
KT (keV)	1.9±0.1	=PN		1.6±0.1	=PN		1.85±0.04	=PN	
Norm bbody	$(4.0^{+5.5/-6.3})\ 10^4$	$(1.7^{+0.8/-0.4})10^6$	**42**	$(7.4^{+1.3/-2.2})10^4$	$(4.5^{+3.7/-1.8})10^6$	**61**	<2.1e2	$(1.5^{+0.3/-0.3})10^6$	**>7e3**
α	3.4±0.1	=PN		3.8±0.1	=PN		3.78±0.01	=PN	
Norm pow	$(5.2^{+3.0/2.1})10^7$	$(1.2^{+0.8/-0.5})10^8$	**2.3**	$(1.1±0.4)10^8$	$(3.5±1.2)10^8$	**3.2**	$(2.3^{+0.5/-0.5})10^8$	$(2.5^{+0.7/-0.8})10^8$	**1.08**
χ^2 (dof)	1.03(1699)	1.00(566)		1.07(1699)	1.12(566)		1.21(1699)	1.01(566)	

Table 4: Spectral analysis results. The fitting model is a blackbody plus a power law.

Fitting MOS and PN with the common model composed of a low energy blackbody and a power law in the range 3-11.5 keV and fixing the spectral index and the temperature to the same value in both spectra gives, we obtain the best-fit parameters listed in Table 4. A blackbody + powerlaw model is a good interpretation of the observed spectra of MOS and PN. While the normalisation of the power-law varies with a factor ranging from 1 to 3 which can be considered consistent with the general uncertainties of the proton response files, the blackbody normalization changes considerably in the two instruments and in different observations of the same instrument. As shown in Table 4, the ratio of the MOS and PN blackbody normalization factors is about 40-60 in the first two observations, while in the third we only find an upper limit for the PN soft excess.

3.4.2 Validation with orbit averaged spectra

The soft proton spectrum detected by the EPIC MOS with the medium filter and extracted from almost 200 ks of observations at a high contamination state, reported in Sect. 1.1, was fitted with a black-body + powerlaw model using the proton response files for MOS medium filter configuration. The presence of a soft excess is also found in the averaged spectrum and we are also able to find a sufficient best-fit (red. χ^2 = 1409/566) only by cutting the spectrum at 3 keV (Fig. 31, left). The best-fit parameters are listed in Table 5. The fit is not optimal because of an additional soft excess that the black-body cannot explain and a bump at 5 keV. Since a dedicated spectral analysis of soft proton flares is outside the scope of this work, we find the best fit model to sufficiently describe - given the general uncertainties of the response files - the observed spectrum.
The best fit model, normalized for the maximum rate observed in 90% of the exposure, is compared with the Solar Wind and the Magnetosheath spectra. The latter are obtained for the maximum flux observed in 90% of operational time of in-flight radiation monitoring data. The result is shown in Fig. 31 (right), with a 50% uncertainty applied to the best-fit model. Both the intensity and slope of the power-law component are in good agreement with the MS model.

Parameter	Value
kT (bbody)	1.75 +/- 0.02
norm (bbody)	(2.5 +/- 0.3) $\times 10^7$
photon index (pow)	3.52 +/- 0.02
norm (pow)	(7.2 +/- 0.1) $\times 10^7$

Table 5: Best fit parameters from the analysis of the MOS spectrum.

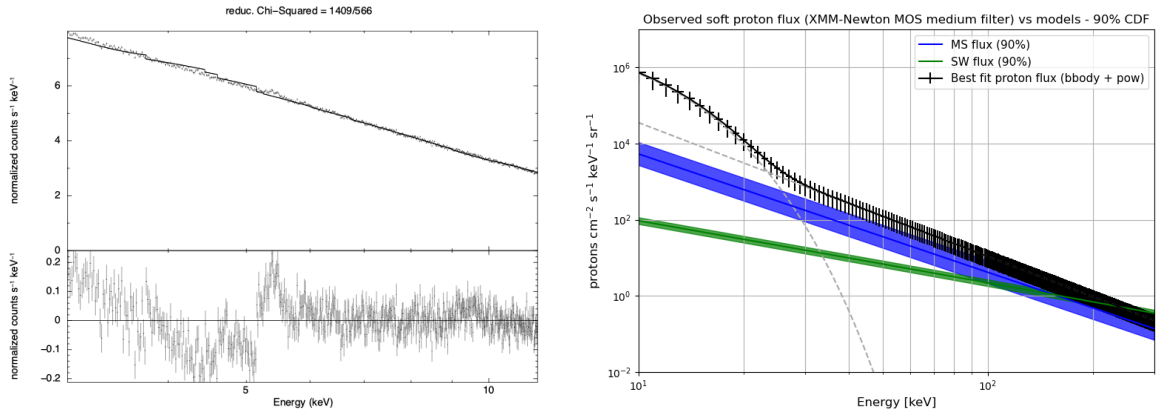

Figure 31: (left) Best fit model of the MOS (medium filter) averaged spectrum obtained from high contamination states. (right) Comparison between the MS and SW input proton models and the best-fit model normalized for the maximum rate observed at 90% of the exposure.

3.4.3 Summary of the validation activity

An actual validation of the proton response files would require generating at the SPO entrance low energy proton beams and measuring on-ground the effect of their transmission through the mirror and the FPA filters. Since this is not - yet - possible, we validated our simulation with in-flight data while in principle not knowing the proton population entering the mirror.
We can state that in general the response files can successfully analyse or simulate the spectra above an observed 5-6 keV lower limit both in terms of the predicted flux and the spectral distribution at the focal plane. Below these energies, we found a soft excess varying between simultaneous MOS and PN observations and with respect to the power-law component. Further studies are required to assess the origin of the soft excess. While it is not the scope of this validation activity to study the origin of XMM-Newton soft proton flares, we could speculate that there is a power-law component that arises above 30-40 keV than is consistent with the proton fluxes measured in the magnetotail. At low energies, we found instead an excess that because of its varying nature could be either linked to additional background components or limitations in the accuracy of the proton response files.

References

[1] Turner, M. J. L. et al., "The European Photon Imaging Camera on XMM-Newton: The MOS cameras," A&A 365, L27–L35 (2001).

[2] Struder, L. et al., "The european photon imaging camera on xmm-newton: The pn-ccd camera," A&A 365, L18–L26 (2001).

[3] den Herder, J. W. et al., "Performance of the reflection grating spectrometer CCD detectors onboard XMM-Newton," Proc. SPIE 5501, 32–43 (2004).

[4] Nartallo, R. et al., "Radiation Environment Induced Degradation on Chandra and Implications for XMM-Newton," Esa/estec/tos-em/00-015/RN Tech. Report (2002).

[5] Jansen, F. et al., “Xmm-newton observatory. i. the spacecraft and operations,” A&A 365, L1–L6 (2001).

[6] Marelli, M. et al., “A systematic analysis of the XMM-Newton background: I. Dataset and extraction procedures,” Experimental Astronomy 44(3), 297–308 (2017).

[7] Molendi, S. et al., “Radiation Background Data Analysis & Lessons Learned from Previous X-ray Missions”, AREMBES WP1 TN 1., 2017

[8] Agostinelli, S. et al., “Geant4–a simulation toolkit,” NIM A 506, 250 – 303 (2003).

[9] Allison, J. et al., “Geant4 developments and applications,” IEEE Trans. Nucl. Sci. 53(1), 270 –278 (2006).

[10] Fioretti, V. et al., “The Geant4 mass model of the ATHENA Silicon Pore Optics and its effect on soft proton scattering”, Proc. SPIE, 106993J (2018)

[11] Diebold, S. et al., “Updates on experimental grazing angle soft proton scattering,” Proc. of SPIE 10397, 103970W (2017).

[12] Fioretti, V. et al., “Geant4 simulations of soft proton scattering in X-ray optics. A tentative validation using laboratory measurements,” Experimental Astronomy 44(3), 413–435 (2017).

[13] Molendi, S. et al., “EXACRAD final report”, ESA Tender (2021)

[14] Fioretti, V. et al., “EXACRAD WP 8.1 final report”, EXACRAD TN (2021)

[15] Henke, B. L., Gullikson, E. M., and Davis, J. C., “X-Ray Interactions: Photoabsorption, Scattering, Transmission, and Reflection at E = 50-30,000 eV, Z = 1-92,” Atomic Data and Nuclear Data Tables 54(2), 181–342 (1993).

[16] Owens, A. et al., “Measuring reflected x-ray absorption fine structure in gold-coated x-ray mirrors,” Proc. of SPIE 2279, 325–331 (1994).

[17] Remizovich, V. S., Ryazanov, M. I., and Tilinin, I. S., “Energy and angular distributions of particles reflected in glancing incidence of a beam of ions on the surface of a material,” Sov. J. Exp. Th. Phys. 52, 225 (1980).

[18] Amato, R. et al., “Soft proton scattering at grazing incidence from X-ray mirrors: analysis of experimental data in the framework of the non-elastic approximation,” Experimental Astronomy 49(3), 115–140 (2020).

[19] Mineo, T. et al., “An XMM-Newton proton response matrix”, Exp. Astr., 44, 3 (2017)

[20] Holland, A. D. et al., “MOS CCDs for the EPIC on XMM,” Proc. of SPIE 2808, 414–420 (1996).

[21] Hiraga, J. et al., “Direct measurement of sub-pixel structure of the EPIC MOS CCD on-board the XMM//NEWTON satellite,” NIM A 465(2-3), 384–393 (2001).

[22] Fraser, G. W. et al., “Potential solar axion signatures in X-ray observations with the XMM-Newton observatory,” MNRAS 445(2), 2146–2168 (2014).

[23] Nandra, K., et al., “The Hot and Energetic Universe: A White Paper presenting the science theme motivating the Athena+ mission”, White Paper (2013)

[24] Meidinger, N. et al., “The Wide Field Imager instrument for Athena,” Proc. of SPIE 10397, 103970V (2017)

[25] Barret, D. et al., “The Athena X-ray Integral Field Unit: a consolidated design for the system requirement review of the preliminary definition phase, Proc. SPIE", 121810L (2022)

[26] Lotti, S. et al., “Soft proton flux on ATHENA focal plane and its impact on the magnetic diverter design”, Exp. Astr. 45, 411–428 (2018)

[27] Fioretti, V. et al. “Magnetic Shielding of Soft Protons in Future X-Ray Telescopes: The Case of the ATHENA Wide Field Imager”, ApJ, 867, 9 (2018)

[28] Athena Study team, “ATHENA - Telescope Reference Design and Effective Area Estimates”, ESA-ATHENA-ESTEC-PL-DD-0001, v3.3, 21/12/2020

[29] Lotti, S. et al., “Review of the Particle Background of the Athena X-IFU Instrument”, ApJ, 909, 111 (2021)

Deliverables

The proton RMF and ARF files are available for download without restriction at the following INAF gitlab repository:

https://www.ict.inaf.it/gitlab/proton_response_matrix

Dissemination & communication activities

Conferences:

- SPIE OP314 (Optics for EUV, X-Ray, and Gamma-Ray Astronomy X) 2021 poster and conference proceeding with the title “Design and characterization of a prototype proton response matrix for the XMM-Newton mission”

Deviations and non-compliances

There are no deviations or non-compliances at the moment. There are however some limitations when using the current release of the proton response files:

- a total uncertainty of 50% must be assigned to any result produced with the response files since many approximations or assumptions were required along the work;
- the MOS is covered by a non-uniform electrode structure that strongly affects the energy redistribution of the protons. While the 60% to 40% surface coverage of the two different electrodes was verified with the measured X-ray transmission, the continuous energy losses in the proton interaction while crossing the read-out device could produce unwanted effects that the Geant4 itself cannot reproduce. Also, small discrepancies in the X-ray transmission could translate into larger differences when considering the proton stopping power.
- The limited statistics of the simulations were underestimated in writing the proposal hence no funding was dedicated to the purchase of run time in external computing services. This led to randomly sampling the proton distribution and using interpolation functions for the energy redistribution, which limited the validity energy ranges of the response files.